Effects of nanocrystallisation on saturation magnetisation of amorphous Fe76Si9B10P5

doi: 10.1080/21663831.2017.1398191

Materials Research Letters

ISSN: (Print) 2166-3831 (Online) Journal homepage: https://www.tandfonline.com/loi/tmrl20

Effects of nanocrystallisation on saturation magnetisation of amorphous $Fe_{76}Si_9B_{10}P_5$

Noriharu Yodoshi, Shunpei Ookawa, Rui Yamada, Naoyuki Nomura, Keiko Kikuchi & Akira Kawasaki

To cite this article: Noriharu Yodoshi, Shunpei Ookawa, Rui Yamada, Naoyuki Nomura, Keiko Kikuchi & Akira Kawasaki (2018) Effects of nanocrystallisation on saturation magnetisation of amorphous $Fe_{76}Si_9B_{10}P_5$, Materials Research Letters, 6:1, 100-105, DOI: 10.1080/21663831.2017.1398191

To link to this article: https://doi.org/10.1080/21663831.2017.1398191

Published online: 07 Nov 2017.

MATER. RES. LETT., 2018
VOL. 6, NO. 1, 100–105
https://doi.org/10.1080/21663831.2017.1398191

MATERIALS RESEARCH LETTERS
Taylor & Francis
Taylor & Francis Group

ORIGINAL REPORT

Effects of nanocrystallisation on saturation magnetisation of amorphous $Fe_{76}Si_9B_{10}P_5$

Noriharu Yodoshi[a], Shunpei Ookawa[b], Rui Yamada[c], Naoyuki Nomura[b], Keiko Kikuchi[b] and Akira Kawasaki[b]

[a]Institute for Materials Research, Tohoku University, Sendai, Japan; [b]Graduate School of Engineering, Tohoku University, Sendai, Japan; [c]Frontier Research Institute of Interdisciplinary Sciences, Tohoku University, Sendai, Japan

ABSTRACT

Amorphous $Fe_{76}Si_9B_{10}P_5$ particles were fabricated by a container-free solidification process and subsequent annealing, and their structural and magnetic properties were investigated by X-ray diffraction analysis, transmission electronic microscopy, and vibrating sample magnetometry. The annealing induced the nanocrystallisation of α-Fe and Fe-B compounds. The proportions of the different crystalline phases formed were dependent on the annealing temperature. The saturation magnetisation of the single particles was higher than that of the samples prepared by a conventional quenching process; this was attributable to the higher homogeneity of the nanocrystalline grains of the former as well as their higher α-Fe to Fe-B compound ratio.

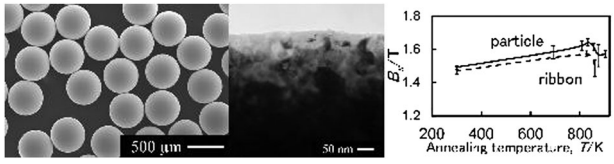

IMPACT STATEMENT

We have investigated single particles obtained by a container-free solidification process to gain deeper insight into their magnetic properties than is possible with samples obtained by conventional processes.

ARTICLE HISTORY
Received 17 August 2017

KEYWORDS
Soft-magnetic materials; amorphous alloys; nanostructured materials; rapid solidification; container-free solidification

Soft-magnetic materials that exhibit high magnetic performance in electronic and power devices have attracted considerable interest for their energy-saving potential and have, therefore, become the focus of extensive research efforts [1,2]. Silicon steel is the most commonly used soft-magnetic material; however, increases in its efficiency based on reductions in its core loss have plateaued [3,4]. Non-equilibrium soft-magnetic materials show lower core losses over a wide frequency range, and this is expected to significantly reduce the energy-conversion losses in the devices based on these materials [5,6]. Materials containing a high density of fine nanocrystalline α-Fe grains within the amorphous matrix have been developed; these materials exhibit lower core losses and higher permeabilities and saturation magnetic flux densities as compared to those of silicon steel [7–9]. Hence, these materials have the potential to replace silicon steel [10,11].

The two primary conventional methods available for fabricating non-equilibrium materials are melt spinning and atomisation [12]. However, the ribbon samples obtained by melt spinning generally exhibit high magnetic anisotropy, while the magnetic properties of atomised powders depend on the compaction density as well as the lubricants and binders added [13–15], making the evaluation of the intrinsic magnetic properties of non-equilibrium materials extremely arduous. Consequently, it has not been possible so far to establish the relationship between the magnetic properties of non-equilibrium materials and the nanostructure of their inner grains.

In this study, we investigated the magnetic properties of a single spherical particle with a homogeneous inner structure. The particle was fabricated by a container-free solidification process called the pulsated orifice ejection method (POEM) [16,17]. With this method, the number of inner nucleation sites is reduced, resulting

CONTACT Noriharu Yodoshi ynoriharu@imr.tohoku.ac.jp Institute for Materials Research, Tohoku University, 2-1-1, Katahira, Aoba-ku, Sendai 980-8577, Japan

in nanocrystalline grains with greater homogeneity after annealing under optimised conditions [18–20]. In addition, the magnetic isotropy of the particle and the absence of perturbing magnetic interactions (due to the absence of other magnetic particles in the vicinity of the particle being investigated) allowed the intrinsic magnetic properties of the material to be evaluated in relation to its nanocrystallisation behaviour. Thus, the hypothesis that the nanocrystallisation of α-Fe in the amorphous matrix increases the saturation magnetisation could be explored.

Amorphous $Fe_{76}Si_9B_{10}P_5$ was selected because this alloy has been reported to have the highest glass-forming ability of all the Fe-based alloy systems [21,22]. First, a master ingot with the nominal composition $Fe_{76}Si_9B_{10}P_5$ was prepared by the induction heating of a mixture of pure elements. Next, monodispersed spherical particles were fabricated by POEM [23,24] and subsequently annealed at different temperatures. The as-fabricated particles were observed using scanning electron microscopy (SEM). Further, they were characterised after annealing by X-ray diffraction (XRD) and transmission electron microscopy (TEM) analyses. The magnetic properties of a single particle were measured with a vibrating sample magnetometer (VSM). A ribbon with a width of 5 mm and thickness of 20 μm as well as a gas-atomised powder consisting of particles less than 45 μm in diameter was prepared and evaluated in the same manner as the single particle, for comparison purposes.

Figure 1(a) shows an SEM image of the as-fabricated monodispersed particles 465 μm in diameter. It can be seen that the particles are highly spherical, have smooth surfaces, and are highly uniform in size.

Figure 1(b,c) shows TEM images of a single particle and the ribbon, respectively. Neither image exhibits a contrast corresponding to a crystal structure nor electron diffraction pattern contains any spots related to a specific diffraction plane.

Differential scanning calorimetry (DSC) measurements were performed before annealing. The Curie, glass transition, and crystallisation temperatures were found to be 691, 784, and 828 K, respectively. Annealing was performed subsequently at 691, 808, 833, 856, 873, and 903 K.

Figure 2(a) shows cross-sectional XRD patterns of the particles annealed at the different temperatures. No peak is observed in the case of the sample annealed at 691 K, while only a very small peak is observed in the case of

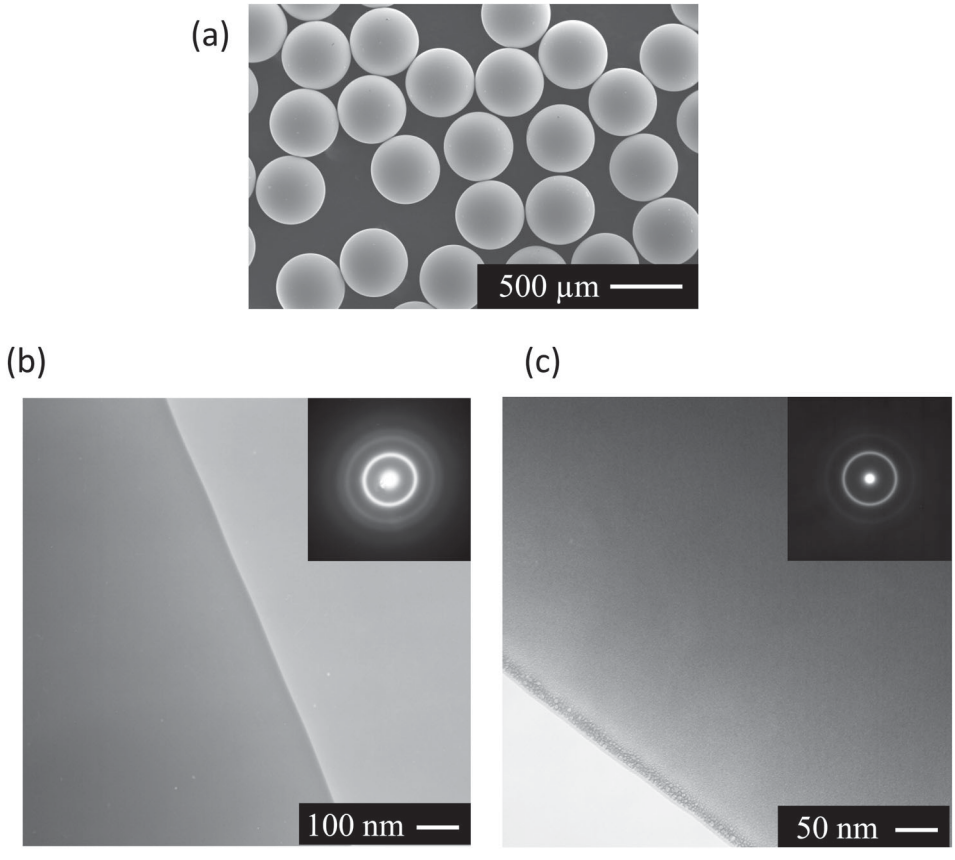

Figure 1. (a) SEM image of monodispersed particles prepared by pulsated orifice ejection method (POEM). (b) TEM image and electron diffraction pattern of the particles. (c) TEM image and electron diffraction pattern of ribbon of same composition.

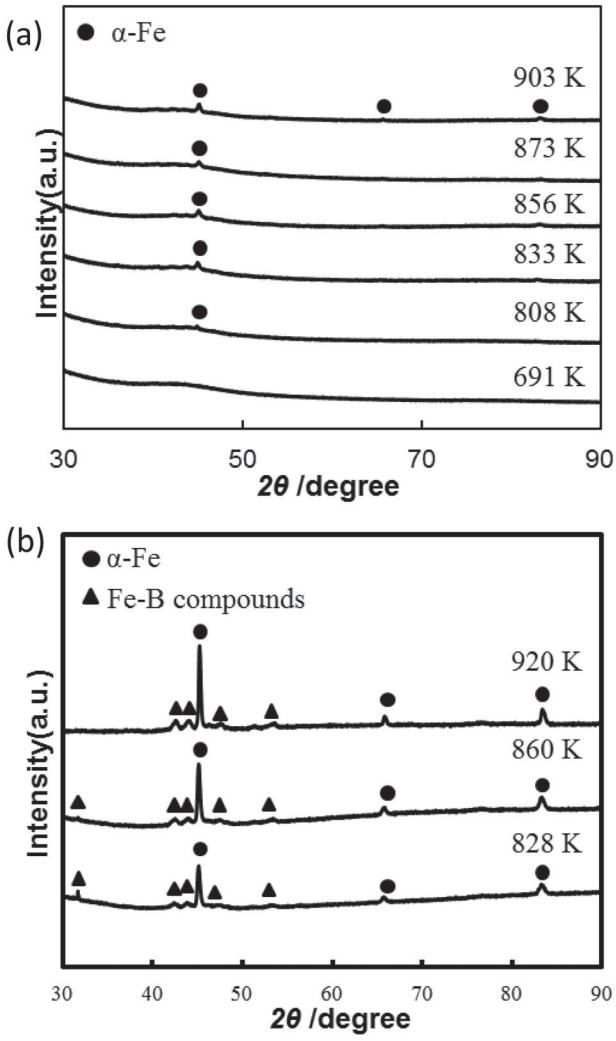

Figure 2. Cross-sectional XRD patterns of (a) particles after annealing treatment at 691, 808, 833, 856, 873, and 903 K, and (b) ribbons after annealing treatment at 828, 860, and 920 K.

the other samples. This peak is attributed to α-Fe, and because its intensity increases with the annealing temperature, it can be concluded that the annealing treatment caused the formation of small crystalline α-Fe grains in the otherwise amorphous $Fe_{76}Si_9B_{10}P_5$ alloy.

On the other hand, Figure 2(b) shows the XRD patterns of the ribbons after they had been annealed at various temperatures. A few Fe-B phase peaks along with α-Fe peaks can be seen clearly in the early stage of annealing. The fact that the first α-Fe peak, which is observed at approximately 45°, increased in intensity with the annealing temperature along with the sharpness (half bandwidth) of the α-Fe peaks indicated that relatively large crystal grains were formed in the amorphous matrix. This is not the early stage of the nucleation process, but the growth stage, in contrast to the case corresponding to Figure 2(a).

Figure 3(a) shows a TEM image and the electron diffraction pattern of a particle annealed at 808 K. Homogeneous nanocrystalline grains approximately 25–30 nm in circle-equivalent diameter can be seen in the TEM image. The electron diffraction pattern shows that these grains consist of not only α-Fe but also Fe-B compounds. Although the size of the nanocrystalline grains in the particle remained constant for annealing temperatures of 808–873 K, the ratio of α-Fe to the Fe-B compounds changed with the annealing temperature, in agreement with previous reports suggesting that α-Fe can transform into Fe_2B and Fe_3B with an increase in the annealing temperature [25]. Through a series of TEM images, it was also observed that the size of the nanocrystalline grains in the particle remained lower compared to that in the ribbon by approximately 40 nm. Figure 3(b) shows the temperature dependence of the number densities of the crystal grains in the particle and ribbon after being annealed at various temperatures, as determined using TEM image analysis. The curve shows the number of crystal grains per unit volume and indicates that the particle precipitates a larger number of grains as a whole. Further, the fact that a peak is observed at approximately 850 K suggested that optimal annealing increases the number density of the crystal grains significantly. From these results, it can be concluded that, in the case of the ribbon sample, crystal grains nucleate in a random manner and subsequently grow in a random order, eventually transforming into a different phase (Fe-B compounds) that is irregular. In the particle, on the other hand, a large number of fine crystal nuclei are formed simultaneously in the amorphous matrix, resulting in a tandem increase in the number of nanocrystalline grains. Thus, the α-Fe phase is not transformed into Fe-B compounds, in contrast to the case for the annealed ribbon samples.

Figure 4(a) shows the B–H curves as measured by the VSM for a single particle, a ribbon, and the gas-atomised powder of the same composition. The saturation magnetisation of the atomised powder is slightly lower than those of the other samples. This can be explained by the higher degree of oxidation of the powder particles owing to their larger surface area. In addition, the permeability of the powder is smaller for high magnetic fields because the interactions between the powder particles are dominant in this case. In the case of the ribbon sample, the steep curve indicates a very high permeability, which is attributable to the fact that the measurement was performed along a longitudinal plane of the thin ribbon. Magnetising ribbon samples in the transverse direction is difficult because of the demagnetising effects. The permeability of the single particle is low, as per the curve shown in Figure 4(a). However, in this case, the curve was corrected using a demagnetisation factor, N, of 1/3, based on

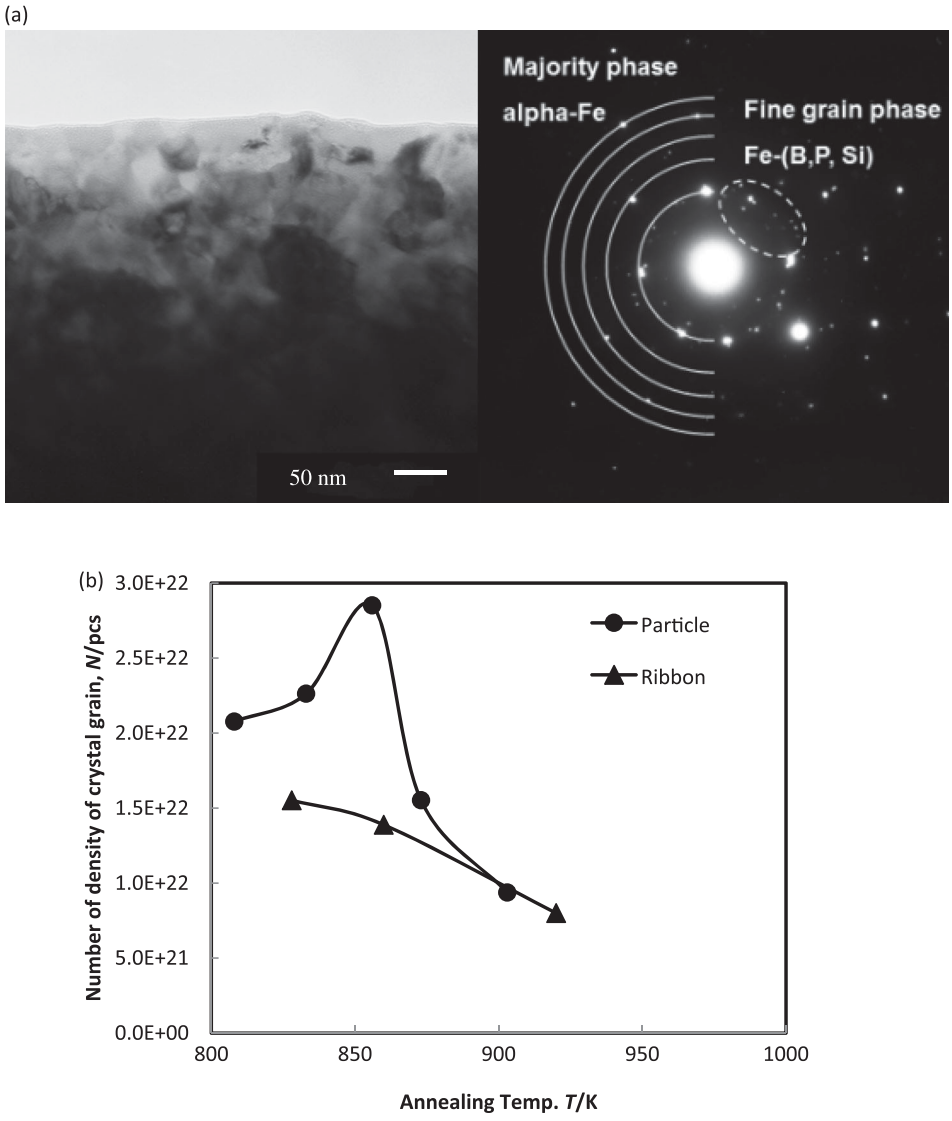

Figure 3. (a) TEM image and electron diffraction pattern of particle annealed at 808 K. (b) Annealing temperature dependence of number density of crystal grains in particle and ribbon after being annealed at various temperatures.

the following equations:

$$H_{\text{eff}} = H - N\frac{J}{\mu_0}, \tag{1}$$

$$B = J + \mu_0 H, \tag{2}$$

where H_{eff}, H, N, μ_0, B, and J are the effective magnetic field, magnetic field, demagnetisation factor, permeability of vacuum, magnetic constant, magnetic flux density, and magnetisation, respectively. The corresponding B–H curve, called the 'after correction' curve, is shown in Figure 4(a) as well. The value of the corrected permeability lies between that of the ribbon as measured along the longitudinal plane and that of the powder. Thus, this result confirms the validity of the measurements performed on this alloy system.

Figure 4(b) shows the annealing temperature dependence of the saturation magnetisation of a single particle as measured by the VSM. Two distinct regions can be observed: in the first region, from the temperature corresponding to no annealing (300 K) to an annealing temperature of 830 K, the saturation magnetisation increases with the annealing temperature, while it decreases in the second region. The first region corresponds to the precipitation of α-Fe grains, as previously observed by TEM. In the case of the second region, the decrease in the saturation magnetisation can be explained by the gradual transition from a ferromagnetic α-Fe phase to a paramagnetic Fe-B compound. The saturation magnetisation of a ribbon sample as a function of the annealing temperature is also shown in Figure 4(b) for comparison. While the saturation magnetisations of both as-fabricated samples

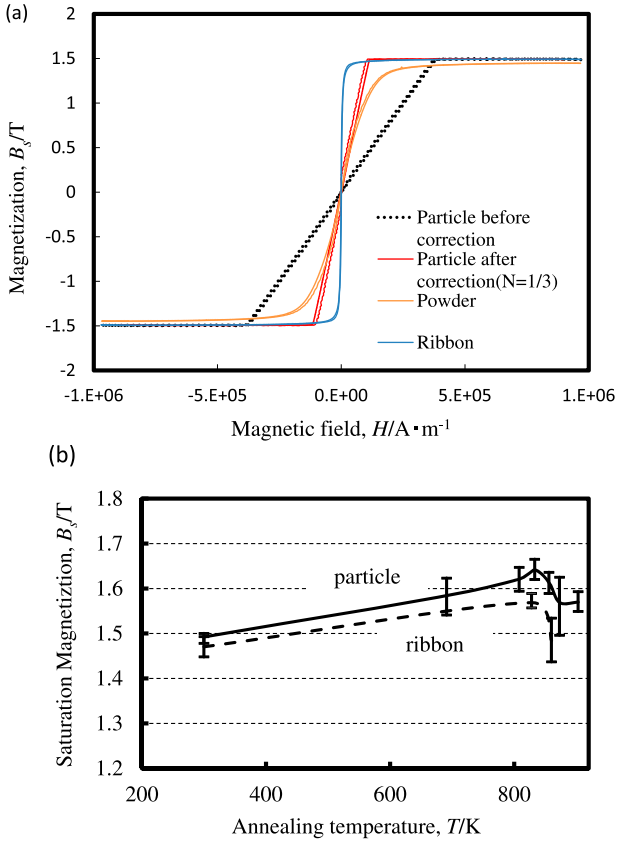

Figure 4. (a) B–H curves of single particle, ribbon, and gas-atomised powder of same composition. (b) Annealing temperature dependence of saturation magnetisation of single particle.

are comparable, the gap between the two curves increases with the annealing temperature, with the maximum saturation magnetisation (corresponding to an annealing temperature of approximately 830 K) for the particle being more than 4% higher than that of the ribbon (1.64 versus 1.57 T). This can be attributed to the higher homogeneity of the nanocrystalline grains (which means a smaller grain size, larger grain number density, and higher volume ratio of the α-Fe phase) of the particle prepared by the container-free POEM, owing to the number of heterogeneous nucleation sites in the case of this preparation method being low. On the other hand, crystallisation in ribbons tends to occur at the contact surface between the sample and the chilled roll during quenching [26]. Consequently, a few α-Fe grains in the ribbon were transformed into Fe-B compounds such as Fe_2B and Fe_3B early in the annealing process, leading to the formation of a greater number of different crystallographic phases than was the case in the particle. This phenomenon is further supported by the XRD results, which confirm the presence of several types of Fe-B compounds in the ribbon after annealing.

Thus, in this study, we investigated the structural and magnetic properties of particles prepared by a container-free solidification process and compared them to those of ribbons obtained by conventional quenching. The obtained results indicated that the uniform nanocrystallisation of α-Fe occurred when the samples were annealed post fabrication. Accordingly, the saturation magnetisation increased with the annealing temperature up to 833 K, while annealing at higher temperatures induced the transformation of α-Fe into Fe-B compounds. This phase transformation was detrimental to the magnetic properties, as evidenced by a decrease in the saturation magnetisation. Similarly, the lower saturation magnetisation exhibited by the ribbons is attributable to a similar phase transformation early in the annealing process. This study demonstrates the feasibility of determining the magnetic properties of a material through single-particle investigations and paves the way for the further development of soft-magnetic non-equilibrium powders as well as the design of novel magnetic devices.

Disclosure statement

No potential conflict of interest was reported by the authors.

Funding

This work was supported by the Japan Society for the Promotion of Science (JSPS) [grant no. 15K18244] and the Materials Science Foundation of Hitachi Metals.

References

[1] Hasegawa R. Present status of amorphous soft magnetic alloys. J Mag Mag Mater. 2000;215–216:240–245.
[2] Suzuki K, Makino A, Inoue A, et al. Soft magnetic properties of nanocrystalline bcc Fe-Zr-B and Fe-M-B-Cu (M = transition metal) alloys with high saturation magnetization. J Appl Phys. 1991;70:6232. DOI:10.1063/1.350006
[3] Hasegawa R. Advances in amorphous and nanocrystalline materials. J Mag Mag Mater. 2012;324:3555–3557.
[4] Kubota T. Recent progress on non-oriented silicon steel. Steel Res Int. 2005;76:464–470.
[5] McHenry ME, Willard MA, Laughlin DE. Amorphous and nanocrystalline materials for applications as soft magnets. Prog Mater Sci. 1999;44:291–433.
[6] McHenry ME, Johnson F, Okumura H, et al. The kinetics of nanocrystallization and microstructural observations in FINEMET, NANOPERM and HITPERM nanocomposite magnetic materials. Scrip Mater. 2003;48:881–887.
[7] Yoshizawa Y, Oguma S, Yamauchi K. New Fe-based soft magnetic alloys composed of ultrafine grain structure. J Appl Phys. 1988;64:6044–6046. DOI:10.1063/1.342149
[8] Kubota T, Makino A, Inoue A. Low core loss of $Fe_{85}Si_2B_8P_4Cu_1$ nanocrystalline alloys with high B_s and B_{800}. J Alloys Comp. 2011;509:S416–S419.

[9] Makino A, Men H, Kubota T, et al. New excellent soft magnetic FeSiBPCu nanocrystallized alloys with high B_s of 1.9 T from nanohetero-amorphous phase. IEEE Trans Magn. 2009;45:4302–4305.
[10] Herzer G. Modern soft magnets: amorphous and nanocrystalline materials. Acta Mater. 2013;61:718–734.
[11] Yoshida S, Mizushima T, Hatanai T, et al. Preparation of new amorphous powder cores using Fe-based glassy alloy. IEEE Trans Magn. 2000;36:3424–3429.
[12] Roy RK, Oanda AK, Mitra A. Alloy development through rapid solidification for soft magnetic application. In: Ahmad Z, editor. New trends in alloy development, characterization and application. Croatia: InTech; 2015. p. 39.
[13] Luan J, Sharma P, Yodoshi N, et al. Mechanically strong nanocrystalline Fe-Si-B-P-Cu soft magnetic powder cores utilizing magnetic metallic glass as a binder. AIP Adv. 2016;6:55934. DOI:10.1063/1.4944766
[14] Kim TH, Jee KK, Kim YB, et al. High-frequency magnetic properties of soft magnetic cores based on nanocrystalline alloy powder prepared by thermal oxidation. J Mag Mag Mater. 2010;322:2423–2427.
[15] Lemieux P, Guthrie R, Isac M. Optimizing soft magnetic composites for power frequency applications and powertrains. JOM 2012;64:374–387.
[16] Fukue M, Yodoshi N, Yamada R, et al. Critical cooling rates of mono-sized Fe-based glassy particles in $[(Fe_XCo_{1-X})_{0.75}B_{0.2}Si_{0.05}]_{96}Nb_4$ system. J Jpn Inst Metals. 2012;76:573–578.
[17] Miura A, Dong W, Fukue M, et al. Preparation of Fe-based monodisperse spherical particles with fully glassy phase. J Alloys Comp. 2011;509:5581–5586.
[18] Herlach DM. Non-equilibrium solidification of undercooled metallic melts. Mater Sci Eng R. 1994;12:177–272.
[19] Wall JJ, Weber R, Kim J, et al. Aerodynamic levitation processing of a Zr-based bulk metallic glass. Mater Sci Eng A. 2007;445:219–222.
[20] Yamada R, Yodoshi N, Kawasaki A. Effects of cooling rates and container walls in preparation of spherical Fe and Pd based metallic glassy particles. J Japan Inst Metals. 2013;77:139–146.
[21] Makino A, Kubota T, Makabe M, et al. FeSiBP metallic glasses with high glass-forming ability and excellent magnetic properties. Mater Sci Eng B-Adv. 2008;148:166–170.
[22] Makino A, Kubota T, Chang CT, et al. Fe-metalloids bulk glassy alloys with high Fe content and high glass-forming ability. Mater Res. 2008;23:1339–1342.
[23] Yodoshi N, Yamada R, Kawasaki A, et al. Evaluation of critical cooling rate of $Fe_{76}Si_9B_{10}P_5$ metallic glass by containerless solidification process. J Alloys Compd. 2015;643:S2–S7.
[24] Yodoshi N, Ookawa S, Yamada R, et al. Temperature dependency of viscosity of $Fe_{76}Si_9B_{10}P_5$ supercooled liquid and hetero-amorphous structure. J Alloys Comp. 2016;679:164–168.
[25] Fornell J, González S, Rossinyol E, et al. Enhanced mechanical properties due to structural changes induced by devitrification in Fe–Co–B–Si–Nb bulk metallic glass. J Acta Mater. 2010;58:6256–6266.
[26] Hennayaka HMMN, Lee HS, Yi S. Surface oxidation of the Fe based amorphous ribbon annealed at temperatures below the glass transition temperature. J Alloys Comp. 2015;618:269–279.